JOURNAL OF NEUROPHYSIOLOGY
Vol. 72, No. 4, October 1994. *Printed in U.S.A.*

Compartmental Models of Type A and Type B Guinea Pig Medial Vestibular Neurons

RETO QUADRONI AND THOMAS KNÖPFEL
Institut für Theoretische Physik, ETH-Hönggerberg, CH-8093 Zurich, Switzerland

SUMMARY AND CONCLUSIONS

1. We have developed compartmental models of guinea-pig medial vestibular nuclei neurons (MVNns). The structure and the parameters of the model cells were chosen to reproduce the responses of type A and type B MVNns as described in electrophysiological recordings.

2. Dynamics of membrane potentials were modeled in 46 and 61 branched electrical compartments for Type A and Type B MVNns, respectively. Each compartment was allowed to contain up to nine active ionic conductances: a fast inactivating sodium conductance, g_{Na}, a persistent sodium conductance, g_{Nap}, a low-voltage activated calcium conductance, $g_{Ca(LVA)}$, a high-voltage activated calcium conductance, $g_{Ca(HVA)}$, a fast-voltage activated potassium conductance, $g_{K(fast)}$, a slowly relaxing voltage activated potassium conductance, $g_{K(slow)}$, a fast transient potassium channel, $g_{K(A)}$, a slowly relaxing mixed sodium-potassium conductance activating at hyperpolarized membrane potentials, g_H, and a calcium-activated potassium conductance $g_{K(AHP)}$. The kinetics of these conductances were derived from voltage-clamp studies in a variety of preparations. Kinetic parameters as well as distribution and density of ion channels were adjusted to yield the reported electrophysiological behavior of medial vestibular neurons.

3. Dynamics of intracellular free $[Ca^{2+}]_i$ were modeled by inclusion of a Ca^{2+}-pump and a Na^+-Ca^{2+} exchanger for extrusion of calcium. Diffusion of calcium between submembraneous sites and the center of an electrical compartment was modeled by 25 and 6 shell-like chemical compartments for the cell body and the proximal dendrites, respectively. These compartments also contained binding sites for calcium.

4. The dynamics of active conductances were the same in both models except for $g_{K(fast)}$. This was necessary to achieve the different shape of spikes and of spike afterhyperpolarization in type A and type B MVNns. An intermediate depolarizing component of the spike afterhyperpolarization of type B neurons in part depended on their dendritic cable structure.

5. Variation of the low threshold calcium conductance, $g_{Ca(LVA)}$, shows that the ability to generate low-threshold spike bursts critically depends on the density of this conductance. Sodium plateaus were generated when increasing the density of g_{Nap}.

6. The type B model cell generated rhythmic bursts of spiking activity under simulation of two distinct experimental conditions. The first experimental condition was the inclusion in the dendritic compartments of a voltage-dependent conductance with properties replicating tonic activation of *N*-methyl-D-aspartate (NMDA)-type of glutamate receptors. The second paradigm was the reduction of the density of $g_{K(AHP)}$. The emergence of oscillatory firing under these two specific experimental conditions is consistent with electrophysiological recordings not used during construction of the model. We, therefore, suggest that these models have a high predictive value.

INTRODUCTION

The vestibulo-oculomotor reflex serves to stabilize the position of the eye with respect to space during movements of the head. The signal initiating this reflex is detected by the semicircular canals and the otoliths. The fundamental component of this reflex involves three neurons: primary vestibular neurons, which carry the signals detected by the semicircular canals and the otoliths; secondary (or central) vestibular neurons; and motoneurons, which innervate the eye muscles. Because of its simplicity and success, the vestibulo-ocular reflex has been chosen as a model in which the function of the central nervous system can be studied both at the cellular and at the system level (Churchland and Sejnowski 1992; Ito 1982; Precht 1978; Robinson 1990). Much previous work has been designated to establish both the inputs to central vestibular neurons and their output. It has been shown that, at the level of the central vestibular neurons, a sensorimotor transformation takes place between the sensory space (plane of semicircular canals and optokinetic input) and the motor space (given by the direction of force developed by the eye muscles) as well as a transformation in the time domain (to achieve proper dynamics). The substrate of these operations relies on the membrane properties, synaptic mechanisms, and connectivity of central vestibular neurons. The network properties emerging from these active membrane properties and synaptic mechanisms are difficult to elucidate without the ideal situation of having access to intracellular recordings from many vestibular neurons simultaneously. During recent years computational methods have become an alternative approach to extrapolate from known cellular properties, synaptic mechanisms and connectivity to network behavior (Koch 1990; Koch and Segev 1989; Traub and Miles 1991).

The aim of the present paper was to construct models of vestibular neurons that should serve as a starting point of such an approach. Among different strategies concerning the type of modeling, we chose the following. First, we decided for a relatively high plausibility of the biophysical mechanisms underlying these models. We used, therefore, Hodgkin-Huxley type of kinetics (Borg-Graham 1991; Hodgkin and Huxley 1952) for voltage-dependent ion channels and Michaelis-Menten type of kinetics for chemical activation of ion channels and detailed modeling of Ca^{2+} dynamics. This approach has the relative disadvantage of being computationally intensive but has the advantage that each parameter could, at least in principle, be related to physiological data. The second decision was to ac-

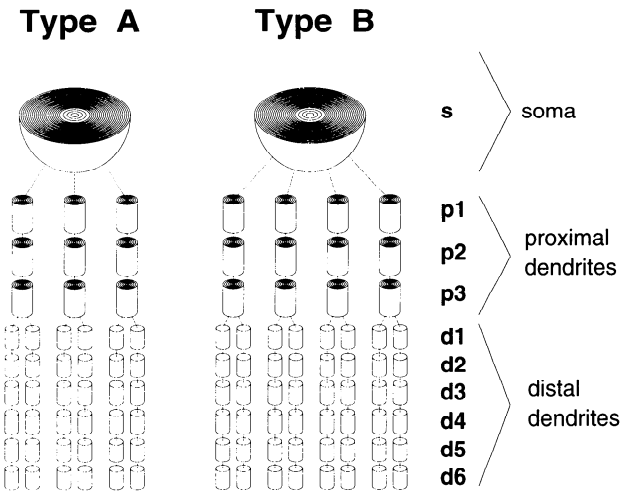

FIG. 1. Compartmental structure of type A and B medial vestibular nuclei neuron (MVNn) models. The type A model has 3 identical branched dendrites and consists of 46 electrical compartments. To calculate radial diffusion of calcium, the soma and the proximal dendrites were discretized into 25 and 6 shell-like chemical compartments. The type B model exhibits the same compartmental structure except for the additional dendrite, which increases the number of electrical compartments to 61.

cept as the most stringent constraints for the value of parameters in the models experimental data from recently published intracellular studies in medial vestibular neurons (Serafin et al. 1990, 1991a,b, 1992). Parameters which were not constrained by these data were additionally constrained by experimental and modeling data from other preparations, in particular from neurons of the deep cerebellar nuclei (Jahnsen 1986a,b; Muri et al. 1994) and hippocampal CA3 pyramidal cells (Traub and Miles 1991).

METHODS

Morphology and electrotonic parameters

Figure 1 shows the structure of the compartmental models for type A and B medial vestibular nuclei neurons (MVNns). The type A MVNn model consisted of a spherical soma which gave rise to three proximal dendrites each of which branched into two distal dendrites. The type B MVNn model had the same overall structure but was endowed with four proximal dendrites. The soma had a radius of 15.5 μm, the radius and length of the proximal dendrite were 1.5 and 99 μm, and the radius and length of the distal dendrites were 0.5 and 198 μm. Proximal and distal dendrites were represented by three and six compartments, respectively, whose electrotonic length was much smaller than 0.1λ (Parnas and Segev 1979). This morphological structure was based on available data from these neurons. In particular, a fourth dendrite was added in the type B model, since type B MVNns seem to have more dendrites than type A MVNns. (M. Serafin, personal communication).

The specific membrane capacitance (C_m) was 1 μFcm^{-2}, and the specific longitudinal (cytoplasmic) resistivity (R_i) was 150 Ωcm. The specific membrane resistivity (R_m) resulted from the contribution of voltage-independent conductances (leak conductances) and active conductances. In the type A model at -65 mV, R_m was $\simeq$3.6 kΩcm^2 in the soma, $\simeq$32 kΩcm^2 in the proximal dendrites, and $\simeq$147 kΩcm^2 in the distal dendrites. The corresponding values for the type B model were $\simeq$3.2 kΩcm^2, $\simeq$37 kΩcm^2, and $\simeq$170 kΩcm^2. R_m values that are higher in the dendrites than in the cell body have been used also in other modeling studies (cf. Shelton, 1985; Traub et al. 1991). Hyperpolarizing current pulses (-0.1 nA) delivered to the cells held at -65 mV revealed an input resistance and time constant of $\simeq$130 MΩ and $\simeq$13 ms in the type A model and $\simeq$150 MΩ and $\simeq$16 ms in the type B model. Values for type A and type B MVNns reported in guinea-pig brain slices are 114.5 MΩ/15.1 ms and 104.5 MΩ/22.4 ms, respectively (Serafin et al. 1991a).

Active membrane conductances

The description of the active conductances was based on the general formalism formulated by Hodgkin and Huxley (1952). Briefly, each channel is controlled by at least one gate and is activated if all gates are open. In most cases, each gate was allowed to be in two states, closed (C) or open (O). The transitions between these states were determined by forward and backward rate functions α and β which depended on membrane voltage (V) and for the calcium-activated potassium channel (see below) also on intracellular Ca^{2+} concentration ($[Ca^{2+}]_i$)

$$\mathrm{C} \underset{\beta(V,[Ca^{2+}]_i)}{\overset{\alpha(V,[Ca^{2+}]_i)}{\rightleftharpoons}} \mathrm{O} \qquad (1)$$

A scheme with two closed states (C_1 and C_2) and one open state (O) was used to describe the inactivation of our low-voltage activated Ca^{2+} conductance

$$\mathrm{C}_1 \underset{\beta_{1,2}(V)}{\overset{\alpha_{1,2}(V)}{\rightleftharpoons}} \mathrm{C}_2 \underset{\beta_{2,3}(V)}{\overset{\alpha_{2,3}(V)}{\rightleftharpoons}} \mathrm{O} \qquad (2)$$

The behavior of a population of channels was described by a state variable, n, for each gate. The value of n lies between 0 and 1 and indicates the fraction of channels with an open gate. In a two-state scheme the dynamics of each variable can be described by a steady-state value, n_∞, and a time-constant, τ_n, both of which depend on voltage and/or on $[Ca^{2+}]_i$

$$\dot{n} = -\frac{n - n_\infty(V,[Ca^{2+}]_i)}{\tau_n(V,[Ca^{2+}]_i)} \qquad (3)$$

The rate of transition from closed to open, $\alpha_n(V, [Ca^{2+}]_i)$, and the rate of transition from open to closed, $\beta_n(V, [Ca^{2+}]_i)$, are related to $n_\infty(V, [Ca^{2+}]_i)$ and $\tau_n(V, [Ca^{2+}]_i)$ by

$$n_\infty(V,[Ca^{2+}]_i) = \frac{\alpha_n(V,[Ca^{2+}]_i)}{\alpha_n(V,[Ca^{2+}]_i) + \beta_n(V,[Ca^{2+}]_i)} \qquad (4)$$

$$\tau_n(V,[Ca^{2+}]_i) = \frac{1}{\alpha_n(V,[Ca^{2+}]_i) + \beta_n(V,[Ca^{2+}]_i)} \qquad (5)$$

For most of the channels, which are only dependent on the membrane voltage, we used the parametrization of Borg-Graham (1991) to describe the rate functions $\alpha_n(V)$ and $\beta_n(V)$

$$\alpha_n(V) \sim \exp(bc(V - V_{1/2})) \qquad (6)$$

$$\beta_n(V) \sim \exp(-b(1 - c)(V - V_{1/2})) \qquad (7)$$

with $b = zF/RT$ (R is the gas constant, T is the temperature, F is the Faraday constant and z is the charge of the gating particle). This formalism requires an additional parameter, $\tau_{n,min}$, which gives a minimum value for $\tau_n(V)$ (Borg-Graham 1991).

The current I flowing through a channel with x activation gates and y inactivation gates was assumed to be ohmic

$$I = \bar{g}m^x h^y (V - E) \qquad (8)$$

where $\bar{g}$ is the conductance of the fully activated channel and E is the Nernst potential of the ion carrying the current. We used this equation also for Ca^{2+} currents, but $E_{Ca^{2+}}$ was set to a value which was lower than that given by the Nernst equation to account for the rectification described by the Goldman-Hodgkin-Katz equation. The rate functions of all channels are given in Table 1.

In the following our choice of rate functions for each channel is explained.

TABLE 1. *Rate functions and parameters to Eqs. 4–8 for the kinetics of active conductances*

Channels and State Variables	Rate Functions: Activation	Rate Functions: Inactivation	Minimal Value for $\tau_n(V)$
g_{Na}	$g_{Na} = \bar{g}_{Na} m^3 h^2$		
m	$\alpha_m = 5.0 \times \exp(0.1 \times (V + 39.5))$	$\beta_m = 5.0 \times \exp(-0.044 \times (V + 39.5))$	$\tau_{min} = 0.05$
h	$\alpha_h = 0.567 \times \exp(-0.024 \times (V + 35.0))$	$\beta_h = 0.567 \times \exp(0.275 \times (V + 35.0))$	$\tau_{min} = 0.3$
g_{Nap}	$g_{Nap} = \bar{g}_{Nap} m$		
m	$\alpha_m = 0.12 \times \exp(0.12 \times (V + 56))$	$\beta_m = 0.12 \times \exp(-0.03 \times (V + 56))$	$\tau_{min} = 1$
g_H	$g_H = \bar{g}_H n$		
n	$\alpha_n = 0.02/(1 + \exp((V + 90)/7.5))$	$\beta_n = 0.02/(1 + \exp(-(V + 90)/7.5))$	
$g^A_{K(fast)}$	$g^A_{K(fast)} = \bar{g}^A_{K(fast)} n^3$		
n	$\alpha_n = 0.16 \times \exp(0.185 \times (V + 42.3))$	$\beta_n = 0.16 \times \exp(-0.033 \times (V + 42.3))$	$\tau_{min} = 0.8$
$g^B_{K(fast)}$	$g^B_{K(fast)} = \bar{g}^B_{K(fast)} n^2$		
n	$\alpha_n = 5.82/(1 + \exp(-0.125 \times (V + 3.3)))$	$\beta_n = 2.413/(1 + \exp(0.0675 \times (V + 46.35)))$	
g_{AHP}	$g_{AHP} = \bar{g}_{AHP} q^2$		
q	$\alpha_q = 3.5 \times 10^9 \times [Ca^{2+}]_i^3$	$\beta_q = 0.074$	
$g_{K(slow)}$	$g_{K(slow)} = \bar{g}_{K(slow)} n$		
n	$\alpha_n = 0.0015 \times \exp(0.156 \times (V + 45.0))$	$\beta_n = 0.0015 \times \exp(-0.039 \times (V + 45.0))$	$\tau_{min} = 80.0$
g_A	$g_A = \bar{g}_A a^3 b$		
a	$\alpha_a = 0.2 \times \exp(0.14 \times (V + 65.0))$	$\beta_a = 0.2 \times \exp(-0.035 \times (V + 65.0))$	$\tau_{min} = 1.0$
b	$\alpha_b = 0.01 \times \exp(-0.11 \times (V + 71.0))$	$\beta_b = 0.01 \times \exp(0.164 \times (V + 71.0))$	$\tau_{min} = 24.0$
$g_{Ca(HVA)}$	$g_{Ca(HVA)} = \bar{g}_{Ca(HVA)} s^2 r$		
s	$\alpha_s = 2.0/(1 + \exp(-(V + 2) \times 0.054))$	$\beta_s = -0.08 \times (V + 15.9)/(1 - \exp((V + 15.9) \times 0.2))$	
r	$\alpha_r = \min(0.01, 0.01 \times \exp(-(V + 60)/20))$	$\beta_r = 0.01 - \alpha_r$	
$g_{Ca(LVA)}$	$g_{Ca(LVA)} = \bar{g}_{Ca(LVA)} m^3 h$		
m	$\alpha_m = 3.3/(1.7 + \exp(-(V + 28.8)/13.5))$		
	$\beta_m = 3.3 \times \exp(-(V + 63)/7.8)/(1.7 + \exp(-(V + 28.8)/13.5))$		
h	$\alpha_{1,2} = 2.5/(t \times (1 + k))$	$\beta_{1,2} = k \times \alpha_{1,2}$	
	$\alpha_{2,3} = 2.5 \times \exp(-(V + 160.3)/17.8)$	$\beta_{2,3} = k \times \alpha_{2,3}$	
	$k = \sqrt{0.25 + \exp((V + 83.5)/6.3)} - 0.5$	$t = 240/(1 + \exp((V + 37.4)/30))$	

For abbreviations, units and explanation see text.

FAST INACTIVATING SODIUM CONDUCTANCE (g_{NA}). Action potentials of type B MVNns are fast (half-width 0.29 ms) (Serafin et al. 1991a) suggesting that g_{Na} exhibits a fast activation. We also assumed a rather fast inactivation to limit the size of outward current required for repolarization of the action potentials. Furthermore, type B MVNns can fire with frequencies of up to 400 Hz, indicating that g_{Na} exhibits a very fast recovery from inactivation (Serafin et al. 1991a,b). Consistent with these assumptions, we found that a m^3h^2 format for g_{Na} was more appropriate than a m^3h dependence. Expressions modifying the m^3h format originally used by Hodgkin and Huxley (1952) to fit the properties of sodium channels of squid giant axon have also been used in a number of previous modeling studies (e.g., Borg-Graham 1991; Traub et al. 1991). The rate functions were adjusted to reproduce as faithfully as possible the shape of the electrophysiologically recorded action potentials.

PERSISTENT SODIUM CONDUCTANCE (g_{NAP}). In addition to g_{Na}, Serafin et al. (1991a) reported the presence of a persistent Na^+ conductance, g_{Nap}, that is responsible for subthreshold plateau potentials. These plateaus do not inactivate during strong depolarization and are differentially sensitive to QX-314 compared with action potentials. Furthermore, long depolarizing pulses can inactivate spikes but not the persistent sodium current (French et al. 1990; Stafstrom et al. 1985). These observations suggest that g_{Nap} is not the window current of g_{Na} but is carried by distinct channels. The persistent sodium channel was modeled with one activation gate using the steady-state activation described by French (1990) on the basis of data obtained in hippocampal pyramidal cells. As suggested by experimental data, we did not include any inactivation of g_{Nap} (French et al. 1990; Stafstrom et al. 1985). Stafstrom found that the persistent sodium current attained its steady state level within 2–4 ms at 37°C. Our activation time was 1 ms at 0 mV and 5 ms at −60 mV.

FAST VOLTAGE-ACTIVATED POTASSIUM CONDUCTANCE ($g_{K(FAST)}$). The only conductance with different kinetics in the type A and type B models was the potassium conductance responsible for repolarization of action potentials. We termed this conductance $g^A_{K(fast)}$ and $g^B_{K(fast)}$ for the type A and B models, respectively. The underlying channel might correspond to the channel termed delayed rectifier in other studies, but $g_{K(fast)}$ might also incorporate other channels such as BK channels (Moczydlowski and Latorre 1983). Type A MVNns exhibit a deep monophasic afterhyperpolarization (AHP), in contrast to type B MVNns, which show a fast AHP followed by a small depolarization and second hyperpolarizing component. In type B MVNns $g^B_{K(fast)}$ must deactivate very fast at the resting membrane potential to allow generation of the small AHP, whereas in type A MVNns $g^A_{K(fast)}$ turns off more slowly and generates the deep AHP. The shape of the action potentials in these cells provided further constraints on the rate functions of $g_{K(fast)}$. In the type B model we used n^2 kinetics that resulted in a fast activation. Together with a high activation threshold, this channel generated very fast action potentials. In type A MVNns we used n^3 kinetics and a lower threshold. As in the case of g_{Na} in previous modeling studies, different exponents (number of gates) have been used to replicate the properties of different potassium channels (e.g., Rudy 1988; Traub et al. 1991). The

resulting delayed activation yielded broader action potentials and the lower threshold caused the deep AHP.

CALCIUM-ACTIVATED POTASSIUM CONDUCTANCE ($g_{K(AHP)}$). The second AHP in the type B MVNn is blocked by apamin, Cd^{2+} and Co^{2+} (de Waele et al. 1993; Serafin et al. 1991a,b) and is, therefore, most likely generated by a Ca^{2+}-dependent K^+ current. A current with similar properties, described in a variety of neurons, is not voltage-dependent, and is usually termed $g_{K(AHP)}$ (Lancaster and Adams 1986; Lancaster and Nicoll 1987; Lancaster et al. 1991). There are several published models of $g_{K(AHP)}$ that are based on different numbers of activation gates and binding sites for intracellular Ca^{2+} (Borg-Graham 1991; Yamada et al. 1989). We used two activation gates, each exhibiting three binding sites for Ca^{2+} ions. The corresponding expression (Table 1) can be interpreted as binding of Ca^{2+} to the channel with Michaelis-Menten-like kinetics (cf. Borg-Graham 1991). The three binding sites for Ca^{2+} ions resulted in a steep Ca^{2+} dependence such that the conductance was not activated at resting calcium concentration (50 nM) but was almost fully activated at a 10-fold higher $[Ca^{2+}]_i$. The kinetics of $g_{K(AHP)}$ were constrained by the ability of our models to exhibit the reported spike accommodation of MVNns.

FAST TRANSIENT POTASSIUM CONDUCTANCE ($g_{K(A)}$). Type A MVNns show a rectification, which delays firing of the neuron. This effect can be explained by the activity of an A-like current, that deinactivates during hyperpolarization and activates rapidly if the cell is subsequently depolarized (Serafin et al. 1991a,b). Segal (1984) described an A-current in hippocampal neurons that is half inactivated at −75 mV, and that recovered from inactivation with a half time of 20 ms at hyperpolarized membrane potentials. Activation of this current was very fast and occurred at potentials higher than −60 mV, and this current was sensitive to 4-AP. However, in MVNns the A-like current was not sensitive to 4-AP (Serafin et al. 1991a). An A-like current, which is not sensitive to 4-AP, and that activates at more hyperpolarized membrane potentials has also been described (Adams et al. 1982). Half inactivation of our $g_{K(A)}$ was set to −71 mV to replicate the slow repolarization of the AHP. The activation time constant was set between 1 and 3 ms and the inactivation time constant was between 24 and 50 ms.

SLOWLY RELAXING VOLTAGE ACTIVATED POTASSIUM CONDUCTANCE ($g_{K(SLOW)}$). In cortical neurons a persistent sodium current is accompanied by a slowly activating outward current (Stafstrom et al. 1985). This slow outward current counteracts the development of sustained Na^+ plateau potentials and shares several properties with the M-current also reported in cortical cells (Brown 1988) but might also partially represent slow depolarization-activated Cl^- currents and currents from electrogenic pumps and exchangers. Since there is no experimental evidence for the existence of M-current in MVNns, we term this slow K^+-current $I_{K(slow)}$. Rather slow kinetics of $I_{K(slow)}$ were required to replicate the observed duration of Na^+-dependent plateau potentials and the relationship between intrasomatically injected current and firing frequency.

SLOWLY RELAXING MIXED SODIUM-POTASSIUM CONDUCTANCE THAT ACTIVATES AT HYPERPOLARIZED MEMBRANE POTENTIALS (g_H). Both types of MVNns showed a sag during injection of hyperpolarizing current pulses. This anomalous rectification is generated by a current that is often termed inward rectifier or I_H. In cat cortical neurons this current is carried by Na^+ and K^+, has a reversal potential of about −50 mV, is half activated between −90 and −80 mV, relaxes with a time constant of about 40 ms at 35°C, and is independent of voltage in the range −60 to −110 mV (Spain et al. 1987). In cerebellar Purkinje cells a similar current activates at potentials more negative than −65 mV, reverses between −56 and −45 mV, and has a relaxation time constant between 52 and 86 ms at 35°C (Crépel and Penit-Soria 1986). The anomalous rectification in type A and B MVNns was eliminated by Cs^+ (Crépel and Penit-Soria 1986; Serafin et al. 1991b; Spain et al. 1987;). Our g_H had a single activation gate, half activation at −90 mV and a voltage-independent time constant of 50 ms. The reversal potential was set to −46 mV by separating g_H into two components permeable for Na^+ ($g_{H,Na}$) and K^+ ($g_{H,K}$), respectively.

TABLE 2. *Density and distribution of ionic conductances for type A and type B models*

	Soma		Proximal Dendrites		Distal Dendrites	
	A	*B*	*A*	*B*	*A*	*B*
$\bar{G}_{Na}$	20172	43000	6667	2880	0	0
$\bar{G}_{Nap}$	33	23.6	32.2	38	0	0
$\bar{G}_H$	110	66	110	66	0	0
$\bar{G}^A_{K(fast)}$	24073	0	6480	0	2430	0
$\bar{G}^B_{K(fast)}$	0	37530	0	2572	0	640
$\bar{G}_{AHP}$	2167	2716	0	0	0	0
$\bar{G}_{K(slow)}$	298	519	240	406	0	0
$\bar{G}_A$	1829	755	427	0	0	0
$\bar{G}_{Ca(HVA)}$	1110	2385	800	1417	350	350
$\bar{G}_{Ca(LVA)}$	0	166	0	651	0	50
$\bar{G}_{Na(leak)}$	30.2	37.8	0.88	0.7	0.88	0.71
$\bar{G}_{Ca(leak)}$	1.33	1.66	0.06	0.065	0	0
$\bar{G}_{Cl(leak)}$	59.6	74.6	1.25	1	1.25	1
$\bar{G}_{K(leak)}$	132.8	166	4.6	3.69	4.6	3.68

For abbreviations, units and explanation see text. $\bar{G}$ indicates maximal conductance per membrane area (μScm^{-2}).

HIGH-VOLTAGE ACTIVATED CALCIUM CONDUCTANCE ($g_{Ca(HVA)}$). We used a high-threshold, inactivating Ca^{2+} conductance, based on the experimental work of Kay and Wong (1987) and the model of the hippocampal pyramidal cell of Traub et al. (1991). Our steady-state activation closely resembled that of Traub et al., however we used a different time-dependence of activation. To account for the fact that the experimental data of Kay and Wong were obtained at room temperature, our time-dependence of activation for potentials between −30 mV and +10 mV varied less with voltage compared with the model used by Traub et al. (1991).

LOW-VOLTAGE ACTIVATED CALCIUM CONDUCTANCE ($g_{Ca(LVA)}$). The burst responses of type B MVNns are reminiscent of those described in thalamic or cerebellar nuclei neurons (Jahnsen and Llinás 1984a,b; Llinás and Mühlethaler 1988a,b; Serafin et al. 1990). The kinetics of the low threshold Ca^{2+}-conductance in the model is based on the experimental work of Coulter et al. (1989) and the model constructed from this data (Wang et al. 1991). We scaled the rate functions from room temperature to 32°C using a Q_{10} of 3.3 and 2.5 for the rate functions describing activation and inactivation (Coulter et al. 1989).

Density and distribution of ionic conductances

We explored different soma-dendritic distributions of ionic conductance densities together with fine-tuning of the rate functions. For each conductance the density was the same in all compartments of the proximal dendrites and all compartments of the distal dendrites. All simulations illustrated in the RESULTS section were obtained with a single set of parameters for the type A MVNn model (Table 2). For type B MVNns the three sets of parameters used were the following: the first defining a standard type B MVNn (Table 2), the second defining a type B MVNn, which could generate low-threshold Ca^{2+} spikes (B+LTS, Table 3), and a third, which was capable of generating Na^+ plateau potentials

TABLE 3. *Density and distribution of ionic conductances for type B + LTS and type B + NAP models. Only parameters that are different from those in the standard type B model are shown.*

	Soma		Proximal Dendrites		Distal Dendrites	
	B+LTS	B+Nap	B+LTS	B+Nap	B+LTS	B+Nap
$\bar{G}_{Nap}$		59.4		86.3		
$\bar{G}_{K(AHP)}$		1921				
$\bar{G}_{Ca(LVA)}$			1607			

For abbreviations, units and explanation see text.

(B+NAP, Table 3). This reflects also the inhomogeneity of type B neurons described by Serafin et al. (1991a,b). The type B+LTS model had a higher value of $g_{Ca(LVA)}$ whereas the type B+NAP model had a higher value of g_{Nap} and a lower value of $g_{K(AHP)}$ than the standard type B model (Table 3).

In the following we explain our choices for the distribution and density of active conductances.

$\bar{g}_{Na}$. The value of $\bar{g}_{Na}$, was constrained by $\frac{dV}{dt}$ during the upstroke of action potentials and by their width. In several types of neurons it has been described that dendrites can generate sodium action potentials (Lacaille et al. 1987; Matsukawa and Prince 1984; Stuart and Sakmann 1994; Traub et al. 1991; Wong et al. 1979). Therefore, and in analogy to the model of a hippocampal CA3 pyramidal cell by Traub et al., we included a small amount of $\bar{g}_{Na}$ in the proximal dendrites. Our values for $\bar{g}_{Na}$ are comparable with those reported in isolated hippocampal cells (Sah et al. 1988).

$\bar{g}_{Nap}$. Comparison of persistent Na^+ currents recorded in slice with those measured in dissociated neurons (French et al. 1990) revealed that g_{Nap} is expressed mainly in the somatic membrane and in the proximal dendritic membrane. The value of $\bar{g}_{Nap}$ was in the range of 10 nS, consistent with the values reported by French (1990) and by Stafstrom et al. (1985) and was adjusted in the type B+NAP model to obtain plateaus as observed in a subpopulation of type B MVNns (Serafin et al. 1991a,b).

$\bar{g}_{K(fast)}$. The values of $\bar{g}_{K(fast)}$ were constrained by the width of the action potentials and by the shape of the AHPs. A relatively high $\bar{g}_{K(fast)}$ was required in the distal dendrites of our type A model to suppress a third phase during repolarization due to longitudinal currents. In the type B model $\bar{g}_{K(fast)}$ was smaller in the dendrites, resulting in a afterdepolarization due to longitudinal currents.

$\bar{g}_{K(AHP)}$. The density of this conductance was adjusted to replicate the second phase of spike AHP in type B neurons and the frequency accommodation observed during injection of long-lasting depolarizing currents. A relatively high value for $\bar{g}_{K(AHP)}$ was required to obtain appropriate frequency accommodation at the beginning of a spike train. This conductance was incorporated only in the somatic membrane as suggested by indirect experimental evidence obtained in hippocampal pyramidal cells (Knöpfel and Gähwiler, 1992).

$\bar{g}_{K(A)}$. In type A MVNns, $g_{K(A)}$ seems to be significant for a second phase of spike repolarization and for the lag in response to depolarizing current pulses superimposed on hyperpolarizing bias current. The value of $\bar{g}_{K(A)}$ in the type A model was chosen to reproduce this behavior; a smaller $\bar{g}_{K(A)}$ was included in the type B model.

$\bar{g}_{K(slow)}$. The value of $\bar{g}_{K(slow)}$ was adjusted to reproduce the reported relationship between the amplitude of intrasomatically injected current and instantaneous frequency (Serafin et al. 1991a) and to support termination of Na^+ plateau potentials in the type B+NAP model.

$\bar{g}_H$. The conductance of g_H was distributed evenly on the soma and the proximal dendrites. The inward rectification seems to be more pronounced in the type A MVNns than in type B MVNns. We accounted for this.

$\bar{g}_{Ca(HVA)}$. Imaging of depolarization induced elevations in intracellular calcium concentration revealed that high-voltage activated calcium channels are expressed in the soma as well as in the dendrites of neurons of the deep cerebellar nuclei cells (Muri et al. 1994). Since these neurons share many properties with MVNns we assumed that the same was true for MVNns and distributed $\bar{g}_{Ca(HVA)}$ on the somatic and dendritic membrane of our models. In the type B models the value of $\bar{g}_{Ca(HVA)}$ was higher than in the type A model, as deduced from the observation that Ca^{2+} spikes are more readily induced in type B MVNns than in type A MVNns in the presence of K^+ channel blockers.

$\bar{g}_{Ca(LVA)}$. Type A MVNns did not exhibit low-threshold Ca^{2+} spikes in the experiments of Serafin et al. (1991a,b). Therefore, we included this conductance only in the soma and in the proximal dendrites of the type B models.

NMDA-type glutamate receptors

NMDA-type glutamate receptors gate a conductance that depends on voltage and extracellular magnesium concentration ($[Mg^{2+}]_o$). A multistate model for this conductance was described by Jahr and Stevens (1990). We implemented a variation of this model that involves a state variable with Hodgkin-Huxley like kinetics describing the voltage-dependent magnesium block of the channel (Ekeberg et al. 1991)

$$I_{NMDA} = \bar{g}_{NMDA} \times n \times (V - E_{NMDA})$$
$$\alpha_{NMDA}(V) = 3 \times \exp(0.035 \times (V + 10))$$
$$\beta_{NMDA}(V) = [Mg^{2+}]_o \times \exp(-0.035 \times (V + 10)) \quad (9)$$

The reversal potential for NMDA currents, E_{NMDA}, was set to 0 mV, and $[Mg^{2+}]_o$ was 2 mM. The time dependence of n is given by *Eqs. 3, 4,* and *5*. The steady-state value of n is of the same form as given by Jahr and Stevens (1990). To compare the behavior of the model with experiments in which NMDA was applied to the bath, we incorporated NMDA-channels in the dendritic membrane (cf. Audinat et al. 1992) with a maximal conductance, $\bar{g}_{NMDA}$, of 2570 $\mu S cm^{-2}$.

Dynamics of intracellular calcium concentration

The calcium-dependent conductance $g_{K(AHP)}$ had a critical influence on the behavior of our model cells (see RESULTS). We, therefore, decided on a relatively plausible modeling of the dynamics of intracellular calcium concentration. Calcium entering the cell was allowed to diffuse and to bind to calcium-binding proteins and was extruded by Ca-ATPase and a Na^+/Ca^{2+}-exchanger. We did not take into account uptake and release of calcium from intracellular organelles (Koch and Segev 1989; Lytton and Sejnowski 1991; Sala and Hernandez-Cruz 1990).

Diffusion in the soma and proximal dendrites was modeled as radial diffusion (Yamada et al. 1989). The volume of the soma was divided into 21 shells of equal volume. The submembraneous shell was further divided into five thin shells of the equal volume and about 0.05 μm thickness. For the proximal dendrites, we used five thin submembraneous shells, each 0.05 μm thick, and a core volume. In the distal dendrites the whole volume of the compartment was used to compute the calcium concentration. We used the value $D = 6 \times 10^{-9}$ cm^2 ms^{-1} for the radial diffusion constant of calcium (Hodgkin and Keynes 1957). Longitudinal diffusion was not taken into account.

TABLE 4. *Parameters used for modeling dynamics of intracellular calcium concentration*

	Soma		Proximal Dendrites		Distal Dendrites	
	A	*B*	*A*	*B*	*A*	*B*
K_{ex}	3.3×10^{-13}	1.32×10^{-12}	3.21×10^{-13}	2.14×10^{-12}	4.85×10^{-13}	3.2×10^{-12}
K_{ATPase}	2.65×10^{-9}	3.97×10^{-9}	6.43×10^{-10}	1.6×10^{-9}	9.6×10^{-11}	1.55×10^{-10}
[B]	0.025	0.025	0.025	0.025	0.025	0.025

For abbreviations, units and explanation see text.

The action of intracellular calcium binding proteins (buffers) was explicitly taken into account. We assumed the buffers to be fixed and not diffusible (Sala and Hernandez-Cruz 1990; Yamada et al. 1989). They were equally distributed in the volume of the soma and dendrites at a concentration of 25 μM. The buffer was assumed to have one binding site. Binding and unbinding was calculated according to the following scheme

$$[Ca^{2+}]_i[B] \underset{b}{\overset{f}{\rightleftarrows}} [Ca^{2+}B] \qquad (10)$$

with $f = 30\ mM^{-1}\ ms^{-1}$ and $b = 0.03 ms^{-1}$ (Sala and Hernandez-Cruz 1990). This corresponds to a binding constant (K_D) of 1 μM.

The description of the Na^+/Ca^{2+}-exchanger used is based on studies of cardiac cells (Kimura et al. 1987; Mullins 1984). The exchanger was assumed to react instantaneously on changes in intracellular calcium. The resulting calcium flux, $j_{Na^+/Ca^{2+}ex}$, was calculated according to

$$j_{Na^+/Ca^{2+}ex} = -k_{ex}([Na]_i^3[Ca^{2+}]_o \exp(E_1 V) - [Na]_o^3[Ca^{2+}]_i \exp(-E_2 V)) \qquad (11)$$

The concentration of extracellular calcium, $[Ca^{2+}]_o$, was 2 mM, extracellular and intracellular sodium concentration, $[Na^+]_o$ and $[Na^+]_i$, were 152 and 7.6 mM, E_1 was 0.01315 and E_2 was 0.0255.

The Ca^{2+}-ATPase had much slower kinetics than the Na^+/Ca^{2+}-exchanger. In variance to other models we have introduced a binding site for calcium. The calcium flux generated by the Ca^{2+}-ATPase, j_{ATPase}, was calculated according to

$$j_{ATPase} = k_{ATPase} n \qquad (12)$$

$$\dot{n} = f[Ca^{2+}]_i(1 - n) - bn \qquad (13)$$

The state variable n denotes the fraction of occupied binding sites. The rate constants f and b were 100 $mM^{-1}\ ms^{-1}$ and 0.005 ms^{-1}, respectively. The steady-state value of j_{ATPase} is (Lytton and Sejnowski 1991)

$$j_{ATPase} = k_{ATPase} \frac{[Ca^{2+}]_i}{[Ca^{2+}]_i + (b/f)} \qquad (14)$$

The noninstantaneous interaction of calcium with the binding site of the Ca^{2+}-ATPase seems to be plausible and avoids the numerical problems introduced by the nonlinearity of $[Ca^{2+}]_i$ in expression *Eq. 14*.

The membrane currents generated by the Ca^{2+}-ATPase and the Na^+/Ca^{2+}-exchanger contributed only to concentration changes. The electrical current caused by these two extrusion mechanisms, was neglected.

The concentration of calcium binding proteins, the capacity of extrusion mechanisms together with our value of the calcium leak were constrained by an assumed resting calcium concentration of 50 to 80 nM and by assuming that less than 5% of the total intracellular calcium was unbound at resting $[Ca^{2+}]_i$ (Neher and Augustine 1992). These parameters are summarized in Table 4.

Calculation of membrane voltage

The dynamics of the membrane voltage in compartment k, V^k, is given by the discretized cable equation

$$c^k \frac{dV^k}{dt} = -\sum_{ion=Na^+,Ca^{2+},K^+,Cl^-} I^k_{ion} - \sum_{j\ next\ to\ k} (V^k - V^l)/\rho^{k,l} - I^k_{syn} - I^k_{exp} \qquad (15)$$

Here c^k is the capacitance of compartment k and the right-hand side represents all currents entering compartment k. These are synaptic currents (I^k_{syn}), currents injected through an electrode (I^k_{exp}), currents flowing from neighboring compartments, l, with voltage V^l along the longitudinal resistance $\rho^{k,l}$ and the ionic currents flowing through the membrane of the compartment which are

$$I^k_{Na^+} = (g^k_{Na(leak)} + g^k_{Na} + g^k_{Nap} + g^k_{H,Na})(V^k - E_{Na^+}) \qquad (16)$$

$$I^k_{Ca^{2+}} = (g^k_{Ca(leak)} + g^k_{Ca(LVA)} + g^k_{Ca(HVA)})(V^k - E_{Ca^{2+}}) \qquad (17)$$

$$I^k_{K^+} = (g^k_{K(leak)} + g^k_{K(fast)} + g^k_{K(slow)} + g^k_{K(AHP)} + g^k_{K(A)} + g^k_{H,K})(V^k - E_{K^+}) \qquad (18)$$

$$I^k_{Cl^-} = (G^k_{Cl(leak)})(V^k - E_{Cl^-}) \qquad (19)$$

The reversal potentials for Na^+ (E_{Na^+}), Ca^{2+} ($E_{Ca^{2+}}$), K^+ (E_{K^+}) and Cl^- (E_{Cl^-}) were 50, 80, −82, and −70mV, respectively. $g_{H,Na}$ and $g_{H,K}$ are the components of g_H carried by Na^+ and K^+.

Numerical methods

The models were implemented on a simulator running under UNIX, having a X-window based user interface that will be described in detail elsewhere. Briefly, the integration routine uses a predictor-corrector algorithm with variable time steps, which is second-order accurate in time and space, consisting of an explicit predictor and an implicit corrector loop. (Cooley and Dodge 1966; Yamada et al. 1989). Simulations were performed on Sun Sparc workstations. About 30,000 simulations were run to find the parameters of these models. The time that is needed for a simulation of 1 s of activity in the models depends on the accuracy of the simulation and activity in the cell. The simulator needed about 14 s on a Sparc 10 for integrating 25 action potentials in the MVNn models. The maximal time step used was 250 μs; during an action potential the step size was reduced to 2 μs.

RESULTS

In a recent series of papers two main types of neurons in the guinea-pig medial vestibular nuclei (Serafin et al. 1990, 1991a,b, 1992) were described and termed type A MVNns and type B MVNns. For ease of comparison of our models with the electrophysiological recordings most of our illustrations directly refer to figures in Serafin et al. (1991a,b).

Figure 2 (cf. Fig. 2 in Serafin et al. 1991a) shows the basic properties of the MVNn models as observed in current

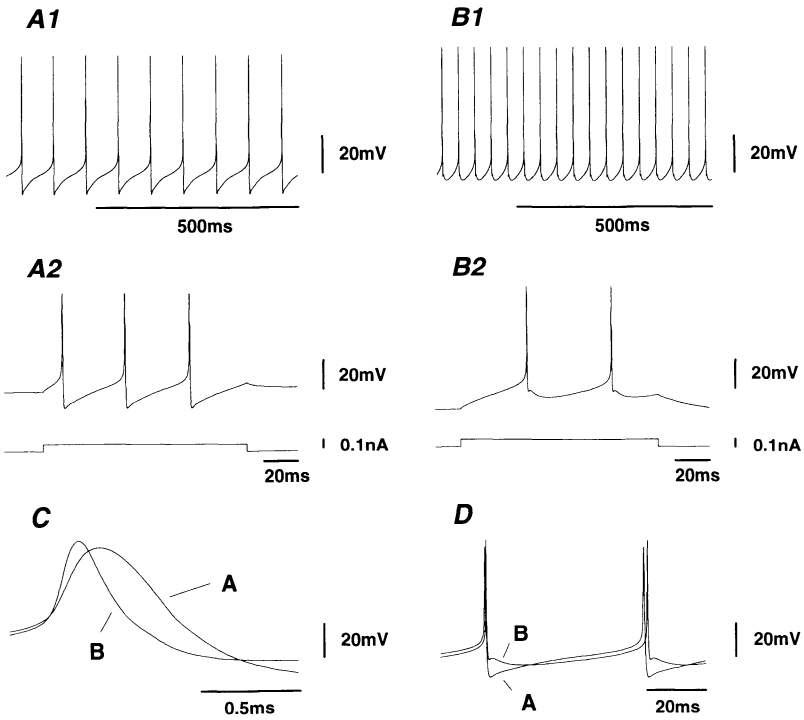

FIG. 2. Basic firing properties of type A and type B MVNn models. *A1* and *B1*: spontaneous generation of action potentials in the type A (*A1*) and type B (*B1*) models. *A2* and *B2*: action potentials induced by depolarizing current pulses (0.09 nA) superimposed on small negative bias currents (−0.04 nA in *A2* and −0.16 nA in *B2*) in the type A (*A2*) and type B (*B2*) models. *C* and *D*: superposition of action potentials and spike afterhyperpolarization (AHP) in the type A (A) and type B (B) models. Note the broader action potential in type A as compared with the type B model, the large monophasic AHP in the type A cell and the biphasic AHP in the type B cell (Fig. 2 cf. Serafin et al. 1991a).

clamp experiments. The type A MVNn and the type B MVNn model exhibited a resting activity which amounted to ≃13 and ≃23 spikes/s, respectively (Fig. 2, *A1* and *B1*). Type A MVNns and type B MVNns have been differentiated according to their width of action potentials and their spike AHP (Serafin et al. 1991a,b). Action potentials of our type A MVN model had a width of ≃0.49 ms and were followed by a single sharp AHP with two phases during repolarization (Fig. 2, *A1, A2, C* and *D*) while our type B model exhibited spikes with a width of ≃0.28 ms and a biphasic AHP (Fig. 2, *B1, B2, C* and *D*). In this respect, our models faithfully reproduce the behavior of MVNns described by Serafin et al. (1991a,b).

The different AHPs were achieved by two distinct fast potassium conductances. In the model of type A MVNn $g^{A}_{K(fast)}$ had a lower threshold for activation and slower kinetics than $g^{B}_{K(fast)}$ in the type B model. To achieve a large dV/dt value during the rising phase of the spike in the type B model, it was necessary to use a higher density of the sodium conductance g_{Na} than in the type A model. In addition, the higher threshold for activation of $g^{B}_{K(fast)}$ favored a large upstroke velocity. Conversely, a lower density of g_{Na} in the type A model and the lower threshold of $g^{A}_{K(fast)}$ resulted in broader action potentials in the type A model. With the exception of the fast potassium conductances all other conductances had the same kinetics in both models. Based on our modeling work, we were able to make the prediction that the two types of cells have different mechanisms causing repolarization of the cell after an action potential. It might, however, be possible that all the other conductances have similar kinetics in both types of cells, since the different behavior of type A and type B cells could be reduced to differences in the distributions of the conductances and in the morphology.

In the following, the behavioral features of our model cells will be described in more detail, and it will be discussed how the various membrane potential responses emerge from the interplay of the different membrane currents.

Membrane currents during electrical activity in the type A model

Figure 3 shows currents flowing through the somatic membrane and between soma and dendrites together with the time course of submembraneous calcium concentration during generation of an action potential. The conductances can be grouped into three classes, according to the magnitude of current they produce during action-potential firing.

As can be seen in Fig. 3, the sharp single-spike AHP of type A MVNns is mainly due to the activation of $g^{A}_{K(fast)}$. The considerable contribution of the longitudinal current, $I_{(long)}$, shows that it is important to include also the morphological structure of the cells. This current tends to slow down the depolarization during an action potential and to depolarize the somatic membrane during the repolarization phase, if the action potential is generated in the soma. Currents with a medium magnitude (Fig. 3*C*) include the current generated by $g_{K(A)}$. The inactivation of $g_{K(A)}$ is partially removed during the deep AHP resulting in the generation of a second phase during the repolarization from the AHP.

The onset of $I_{K(AHP)}$ is delayed with respect to the onset of the action potential. The reason for this is a delayed rise in the intracellular calcium concentration (Fig. 3*A*) caused by activation of the high-voltage activated calcium current $g_{Ca(HVA)}$. Only small currents are generated by $g_{K(slow)}$, g_{Nap}, and g_{H}. The tonic component in the activation of the persistent sodium conductance is responsible for the spontaneous activity of this model cell.

The action of g_{H} is more clearly revealed with hyperpolarizing current pulses injected into the soma of the model cell (Fig. 4, *A* and *B*). Under this condition g_{H} generates an

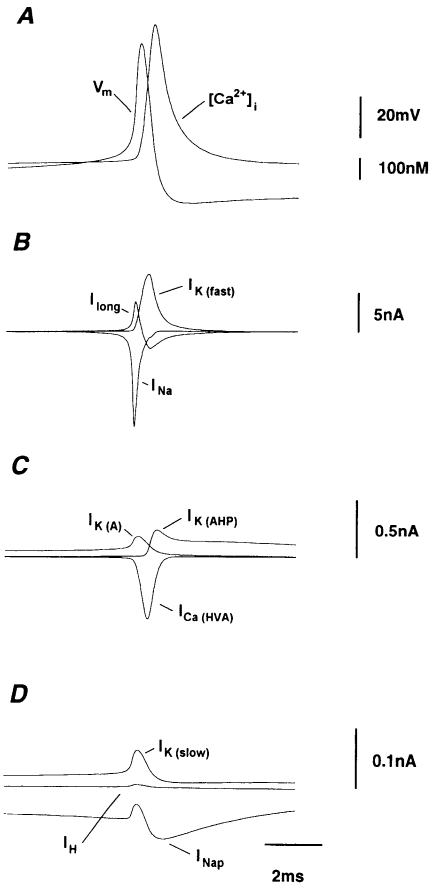

FIG. 3. Active membrane currents flowing through the somatic membrane and between the soma and the dendrites and dynamics of submembraneous calcium concentration during generation of an action potential in the type A model. *A*: membrane potential (V_m) and submembraneous calcium concentration ($[Ca^{2+}]_i$). *B*: currents generated by $g_{K(fast)}$ ($I_{K(fast)}$), g_{Na} (I_{Na}), and current flowing between soma and dendrites (I_{long}). *C*: currents generated by $g_{K(A)}$ ($I_{K(A)}$), $g_{K(AHP)}$ ($I_{K(AHP)}$), and $g_{Ca(HVA)}$ ($I_{Ca(HVA)}$). *D*: currents generated by $g_{K(slow)}$ ($I_{K(slow)}$), g_H (I_H), and g_{Nap} (I_{Nap}). Note that scaling of currents is different in *B*, *C*, and *D*.

inward rectification that is small at the beginning of the hyperpolarization and reaches its maximum after about 250 ms (cf. Fig. 8 in Serafin et al. 1991a). Suprathreshold depolarizing current pulses superimposed on a hyperpolarizing bias current reveal the action of $g_{K(A)}$ (Fig. 4*C*). With this protocol, induction of action-potential firing is delayed due to the transient outward current produced by $g_{K(A)}$ (cf. Fig. 3*D* in Serafin et al. 1991a). Following depolarization from a more hyperpolarized membrane potential, both g_H and $g_{K(A)}$ are transiently activated. In the example illustrated in Fig. 4*D* (cf. Fig. 3*B* in Serafin et al. 1991a) the activity of $g_{K(A)}$ overcomes that of g_H resulting in a delay before generation of the next action potential (see arrow in Fig. 4*D*).

The frequency of action-potential firing, as a function of the strength of current injected into the soma, is a global indicator for the input-output relationship of a neuron. Due to different time-dependent processes, the instantaneous frequency (given by the inverse of the interspike interval) is different for the first, second, and last interspike interval of a spike train induced by a long-lasting depolarizing current pulse. Figure 5 shows the current-frequency plot (FI-plot) obtained with the type A model. This plot closely resembles that shown in the electrophysiological study of Serafin et al. (cf. Fig. 9, 1991a). The conductance producing the frequency accommodation at the beginning of a spike train is $g_{K(AHP)}$ in both models. Since $g_{K(AHP)}$ is calcium-dependent, the FI-relationship is strongly influenced by the dynamics of the intracellular calcium concentration. In the type A model the instantaneous frequency of the second interval is faster than that of the first interval for currents exceeding 0.5 nA. This is caused by a considerable activation of $g_{K(AHP)}$ following the first spike. The spike amplitude decreases during the first 5 spikes, which results in a reduced influx of calcium and, consequently, a reduced activation of $g_{K(AHP)}$. A similar decrease of the spike amplitudes at the beginning of a depolarizing current injection was also reported in the electrophysiological experiments (cf. Fig. 9, *A1* and *A2* in Serafin et al. 1991a). Frequency accomodation is supported by an accumulation of intracellular calcium that causes an additional activation of $g_{K(AHP)}$. Notably, deactivation of $g_{K(AHP)}$ is slowed down during periods of elevated calcium levels between the action potentials. The gradual build-up of $g_{K(slow)}$ significantly contributes to the frequency accommodation at a later phase of a spike train. The contribution of $g_{K(A)}$ during the first intervals is small in this experimental protocol, since the cell was not depolarized from a hyperpolarized potential.

Membrane currents during electrical activity in the type B model

Figure 6 shows all active somatic membrane currents together with the time course of submembraneous calcium concentration during spontaneous generation of an action potential in the type B model. In contrast to the single sharp spike AHP observed in type A MVNns, type B MVNns exhibited a two-component spike AHP, which in our models was generated by the interplay of currents generated by $g^B_{K(fast)}$, $g_{K(AHP)}$ and currents flowing between the cell body and the dendrites. The first component of spike AHP is mainly generated by $g^B_{K(fast)}$, while the second component results from the action of $g_{K(AHP)}$. The latter conductance activates only after repolarization of the action potential, since the submembraneous calcium concentration is delayed compared to the voltage. The depolarizing component between these two hyperpolarizing potentials depends on the dendritic cable structure of the model. Several properties of the different conductances are required to get this characteristic shape of the AHP. As mentioned above, the fast potassium conductance must deactivate very fast near the resting membrane potential, but develops its full power during the repolarization phase. A very fast repolarization of the spike is needed to induce a large potential gradient between the soma and the proximal dendrites (Storm et al. 1987). Due to this gradient, depolarizing currents will flow into the soma until the gradient vanishes. The tail of this compensatory current causes the small afterdepolarization between the two AHPs.

The influx of calcium is caused by the high-voltage activated conductance $g_{Ca(HVA)}$. Almost no current flows through the $g_{Ca(LVA)}$ conductance, due to the inactivation of

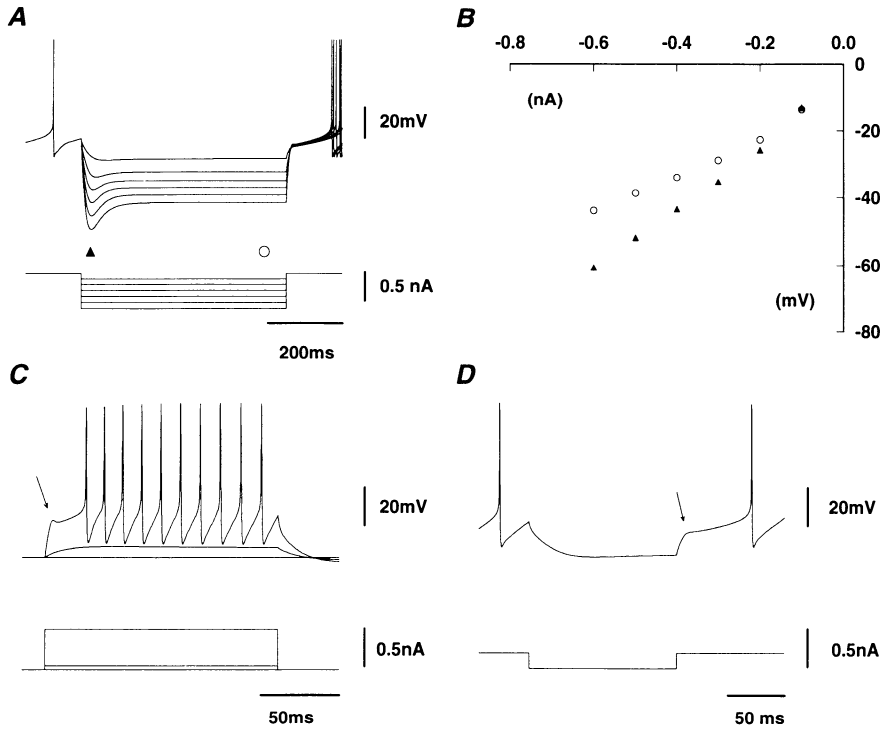

FIG. 4. Action of g_H and $g_{K(A)}$ in the type A model. *A*: intrasomatic injection of hyperpolarizing current pulses (−0.1 to −0.6 nA) reveals slowly developing inward rectification due to activation of g_H. *B*: current-voltage relationship measured at times as indicated in *A* (▲ and ○: shortly and about 500 ms after onset of hyperpolarizing current pulse, see arrows). *C*: action potential firing induced by a depolarizing current pulse superimposed on a hyperpolarizing bias current (−0.17 nA). *D*: transient depression of action-potential firing during a hyperpolarizing current pulse (bias current 0.05 nA). The arrow in *C* and *D* indicates a notch preceding onset of action-potential firing due to the activity of $g_{K(A)}$.

this conductance at potentials near the resting membrane potential. The amount of calcium flowing into the cell during an action potential is about the same as in the type A model, despite the more than two times higher maximal conductance of $g_{Ca(HVA)}$ in the type B model. The broader action potential of the type A cell allows for a higher activation of this conductance and hence a smaller maximal conductance is needed.

The other conductances generate only small currents during an action potential. However, these conductances have a significant influence on the active membrane properties at a slower time scale as it is expressed in the FI-plot (see below). Thus, as in the type A model, g_{Nap} supports spontaneous activity in the type B model. The slow potassium conductance builds up during long-lasting depolarizing current injections. During spontaneous activity it regulates the activity of the cell opposing the action of the persistent sodium conductance. In the type B model g_A does not reach values as high as in the type A model. As a consequence, the type B model does not exhibit a significant delay before generation of an action potential after a long lasting hyperpolarization as it is seen in the type A model (cf. Fig. 4*C*).

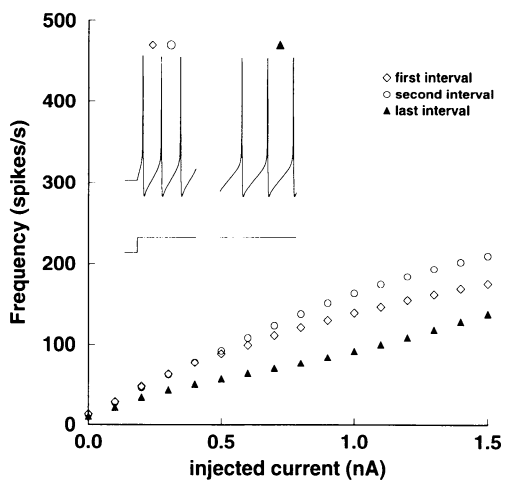

FIG. 5. Relationship between firing frequency and injected current in the type A model. The instantaneous firing frequency was determined as the inverse of the first (◇), second (○), and last (▲) interspike interval of a spike train induced by long lasting (≥1.2 s) depolarizing current pulses, superimposed on a small negative holding current (−0.05 nA). Note, that for large currents, the second interspike interval is shorter than the first one.

Interestingly, the morphology had a marked influence on the shape of the AHP. This can be demonstrated by varying the number of dendrites (Fig. 7). With a reduced number of dendrites the amplitude of the spike and AHP increases due to the decreasing longitudinal currents flowing between the soma and dendrites. With no dendrites there is a monophasic AHP.

The significance of $g_{K(AHP)}$ for the second component of the AHP can be clearly seen when $g_{K(AHP)}$ is set to 20 percent of its standard value (Fig. 8). The resulting voltage trace closely resembles that obtained when $g_{K(AHP)}$ was blocked by apamin in type B MVNns (de Waele et al. 1993).

Finally, our model of type B MVNns faithfully reproduces the described FI-plot (cf. Fig. 9 in Serafin et al. 1991a). The instantaneous frequency in the first interval is dominated by the action of $g_{K(AHP)}$ and to a lesser extent by $g_{K(A)}$. Following the first few spikes of a spike train, build-up of the slow potassium conductance causes a significant contribution to the frequency accommodation. With increasing amplitudes of the injected current, the second AHP disappears, strongly increasing the instantaneous frequency. This leads to a secondary range in the FI-plot for the first interval. Contrary to the type A MVNns, the instantaneous frequency decreases monotonically with time. In the experiments, as well as in the models, no decrease in the amplitudes of the action potentials is seen (Fig. 9, *B1* and

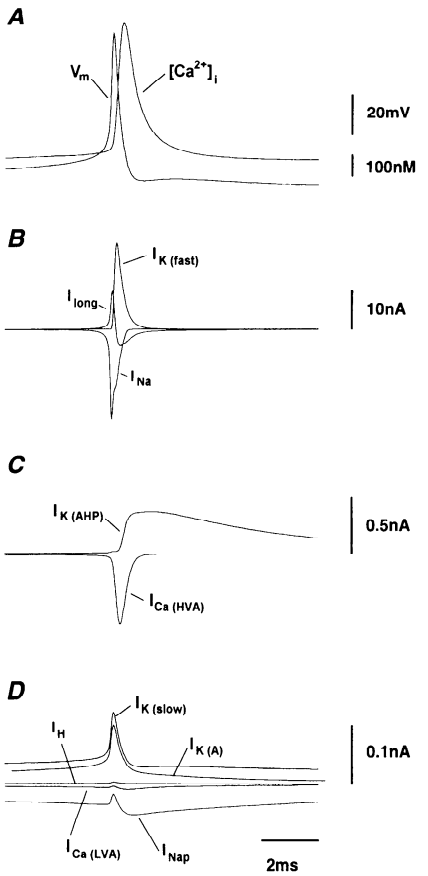

FIG. 6. Currents and dynamics of submembraneous calcium concentration during generation of an action potential in the type B model. *A*: membrane potential (V_m) and submembraneous calcium concentration ($[Ca^{2+}]_i$). *B*: currents generated by $g_{K(fast)}$ ($I_{K(fast)}$), g_{Na} (I_{Na}), and current flowing between soma and dendrites (I_{long}). *C*: currents generated by $g_{K(AHP)}$ ($I_{K(AHP)}$) and $g_{Ca(HVA)}$ ($I_{Ca(HVA)}$). *D*: currents generated by $g_{K(slow)}$ ($I_{K(slow)}$), g_H (I_H), $g_{Ca(LVA)}$ ($I_{Ca(LVA)}$), $g_{K(A)}$ ($I_{K(A)}$), and g_{Nap} (I_{Nap}). Note that scaling of currents is different in *B*, *C*, and *D*.

B2, cf. Serafin et al. 1991a), and hence the influx of calcium is about the same during every action potential.

Type B MVNns exhibiting low-voltage activated spike bursts

A subpopulation of MVNns has been described to exhibit low-voltage activated (LVA) spike bursts (Serafin et al. 1990, 1991a). In our standard type B model the density of $g_{Ca(LVA)}$ was too low to actively generate LVA bursts, which were, however, seen when increasing the density of $g_{Ca(LVA)}$. Figure 10 shows LVA bursts in our type B+LTS model. This higher value of $\bar{g}_{Ca(LVA)}$ did not significantly affect the shape of the action potential or the spike AHP, but the frequency was slightly increased due to the additional depolarizing Ca^{2+} currents in the proximal dendrites (not illustrated).

Type B MVNns exhibiting Na^+-dependent plateau responses

Another portion of MVNns was able to produce Na^+-dependent plateau responses (Serafin et al. 1991a,b). Again, our standard type B model did not actively generate these plateau responses. They could, however, be reproduced

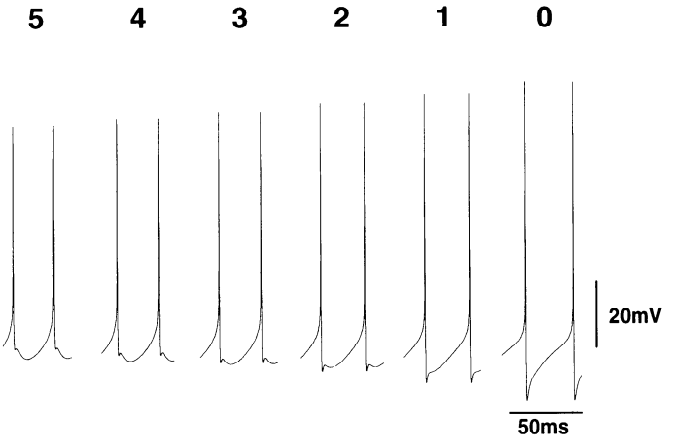

FIG. 7. Effects of varying the number of dendrites in the type B model. Somatic voltage traces from left to right show spontaneous action potentials and AHPs with 5, 4, 3, 2, 1, or 0 dendrites attached to the cell body of the type B model.

when increasing $\bar{g}_{Nap}$ and slightly decreasing $\bar{g}_{K(AHP)}$. Figure 11 shows the Na^+-dependent plateau responses in our type B+NAP model (Serafin et al. 1991a).

Rhythmic burst firing

Two experimental protocols have been reported that can bring about rhythmic burst firing in type B MVNns. The first experimental paradigm involves activation of NMDA-type of glutamate receptors (Serafin et al. 1992). The second condition under which membrane potential oscillations emerge is the application of apamin (de Waele et al. 1993), which blocks $g_{K(AHP)}$. Both processes are potentially of functional significance, because NMDA receptors as well as the Ca^{2+}-activated potassium conductance $g_{K(AHP)}$ are dynamically controlled by neurotransmitters. A small hyperpolarizing current needed to induce the rhythmic burst firing in both experimental situations (de Waele et al. 1993; Serafin et al. 1992) could be provided by synaptic inputs.

These electrophysiological observations were not used to constrain the parameters of the models and could, therefore, be used to validate their predictive utility. The behavior of the standard type B model, under the experimental protocols described above, is shown in Figs. 12 and 13. The

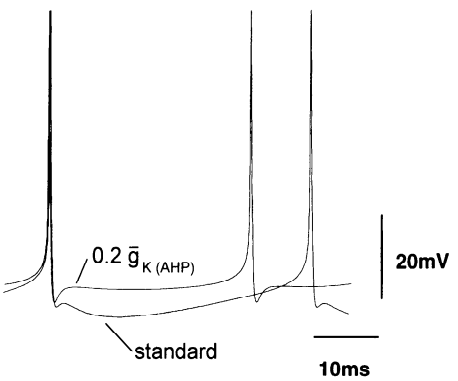

FIG. 8. Effect of lowering $\bar{g}_{K(AHP)}$ in the type B model. The two superimposed traces were obtained with the standard type B model (standard) and with the same parameters except for $\bar{g}_{K(AHP)}$ set to 20% of its standard value (0.2 $\bar{g}_{K(AHP)}$). Note the depression of the second AHP with depression of $g_{K(AHP)}$.

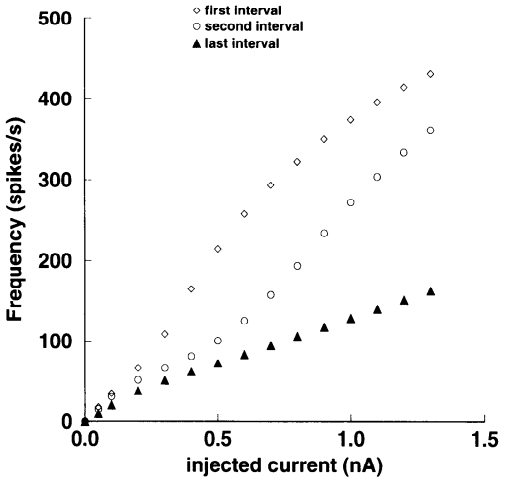

FIG. 9. Relationship between firing frequency and injected current in the type B model. The instantaneous firing frequency was determined as the inverse of the first (◇), second (○), and last (▲) interspike interval of a spike train induced by long lasting (≥1.2 s) depolarizing current pulses superimposed on a small negative holding current (−0.12 nA).

standard type B model exhibits a regular firing pattern, and with injection of hyperpolarizing currents of increasing amplitudes the firing frequency decreases until firing terminates. Thus, as in the electrophysiological recordings (de Waele et al. 1993; Serafin et al. 1992) hyperpolarizing current injections fail to induce bursts under control conditions.

However, with a steady activation of NMDA-receptors in the proximal dendrites the model exhibited a rhythmic burst firing with inter-burst intervals that strongly depended on the amount of hyperpolarizing current injected into the cell. In the model the slow potassium conductance

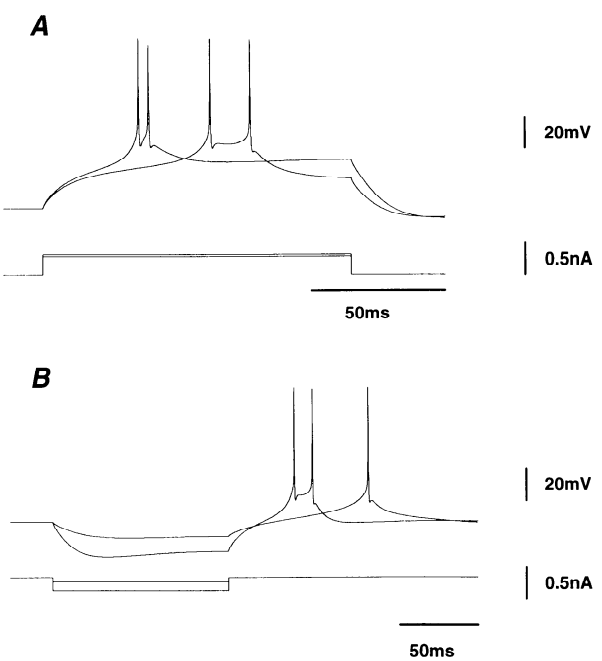

FIG. 10. Low-voltage activated calcium spikes in the type B+LTS model. *A*: low-voltage activated calcium spikes induced by depolarizing current pulses superimposed on a negative bias current. *B*: generation of low-voltage activated calcium spikes following transient hyperpolarization. Holding current was −0.5 nA in *A* and −0.16 nA in *B*.

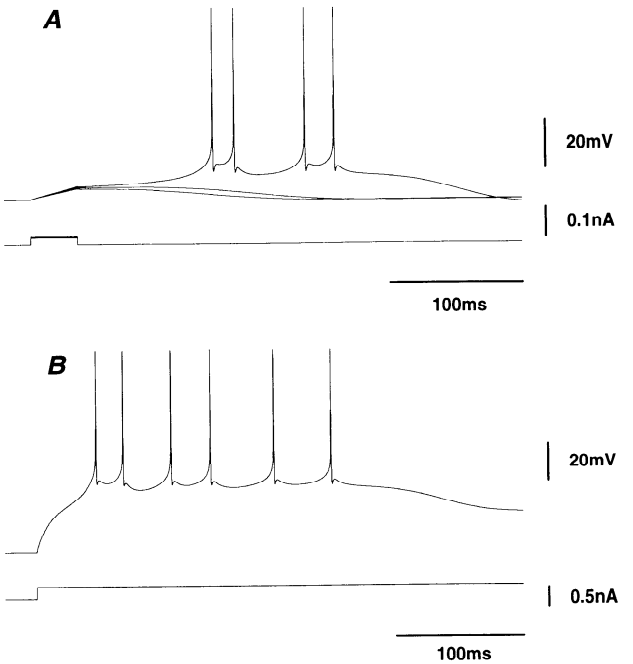

FIG. 11. Plateau potentials generated by g_{Nap} in the type B+NAP model. *A*: long-lasting plateau responses evoked by short-lasting depolarizing current pulses superimposed on a −0.18 nA holding current. *B*: plateau responses induced by switching the holding current from −0.48 nA to −0.18 nA.

$g_{K(slow)}$ accounts for the termination of a burst since its activity builds up during a spike train until it is strong enough to terminate a burst. During the hyperpolarization phase, deactivation of $g_{K(slow)}$ leads to a slow depolarization of the cell until a potential is reached at which the voltage-dependent NMDA channels activate sufficiently for induction of new burst.

Figure 13 shows rhythmic bursting of the type B model with $g_{K(AHP)}$ set to zero a situation corresponding to the electrophysiological experiments with apamin (de Waele et al. 1993). Again, the burst frequency and duration decreases with increasing hyperpolarizing current injection. The mechanism responsible for termination of the bursts is the same as in the NMDA experiment, while g_{Nap}, g_H, and $g_{Ca(LVA)}$ contribute to the depolarization inducing a new burst.

DISCUSSION

In the present paper, we describe models of type A and type B MVNns in the guinea-pig. As the most stringent constraint for the adjustment of parameters we used the data provided by Serafin et al. (1991a,b). The properties of our models might therefore deviate from those described in neurons in vestibular nuclei other than the MVN or in other species. However, we expect that the present models can easily be modified to replicate the behavior of vestibular neurons in other species or neurons of the deep cerebellar nuclei, which share many functional properties with MVNns.

Our models faithfully reproduced the published electrophysiological behavior of these cells as described in current-clamp recordings. Properties of type B MVNns, which are not consistently seen in each neuron recorded (LVA bursts,

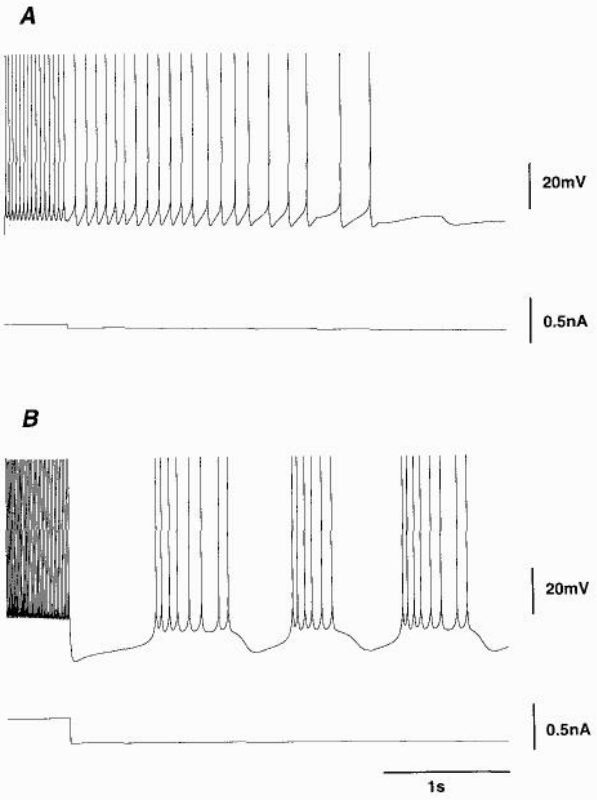

FIG. 12. Tonic activation of *N*-methyl-D-aspartate (NMDA) receptors causes rhythmic bursts of spiking activity in the standard type B model. *A*: regular firing in the absence of NMDA receptor activation. Injection of a step-wise incremented amount of hyperpolarizing current caused a reduction of firing frequency but did not affect the regular firing pattern. *B*: with tonic activation of dendritic NMDA-receptors the model cell exhibited a rhythmic bursting activity during hyperpolarizing current injections (−0.28 nA).

plateau responses), could be reproduced by changing the density of some ionic channels in the models. In addition, the predictive potency of these models was verified by demonstrating their ability to exhibit some properties (oscillations induced by NMDA-receptor activation or depression of $I_{K(AHP)}$) that were not used to tune the parameters of the models.

During the modeling work it turned out that for both models at least nine different conductances, each of which represents a functional class, are required to reproduce all the experimental observations. For instance, it is conceivable that $g_{K(fast)}$ is—with respect to its influence on the electrical behavior—represented on the molecular level by the combined action of a delayed rectifier and an I_c. The kinetics of eight of the implemented conductances were equal in both models. Only the kinetics of the fast potassium conductance, $g_{K(fast)}$, had to be different in the two models to reproduce the different widths of action potentials and the different shape of spike AHP. With the exception of this conductance, only the distribution of the conductances and the morphological structure differ in the two models. In type A MVNns the fast potassium conductance generates a deep AHP that has interesting consequences for the integrative properties of the cell. Immediately after an action potential the membrane potential is much more negative than the threshold of the fast sodium conductance. This opposes high-frequency firing, as can be seen in the FI-plot. In addition, the expression of an A-conductance causes a delay before firing the next action potential. These properties support a regular firing of the cells even with a fluctuating synaptic drive.

On the contrary, the initial AHP component in type B MVNns is small and the fast potassium conductances in these cells seem to deactivate rather quickly. These properties support firing at high frequencies. Immediately after an action potential the membrane potential settles to a value at which several small conductances are activated. This provides a basis for modulation of the excitability of the cell. The most significant of these conductances is the AHP conductance, which is responsible for the second delayed AHP. In the FI-plot this conductance is responsible for the secondary range in the instantaneous frequency related to the first interval. Blocking this conductance changes the excitability of the cell drastically and can induce oscillatory firing patterns. Notably, this conductance is modulated by neurotransmitters in many cell types.

These different intrinsic properties of type A and type B MVNns might correspond to the segregation of MVNns into tonic and phasic neurons (Shimazu and Precht 1965), with the excitability of the phasic neurons being under neuromodulatory control.

The ultimate goal of this work is to provide models of MVNns that can be incorporated into a network model of

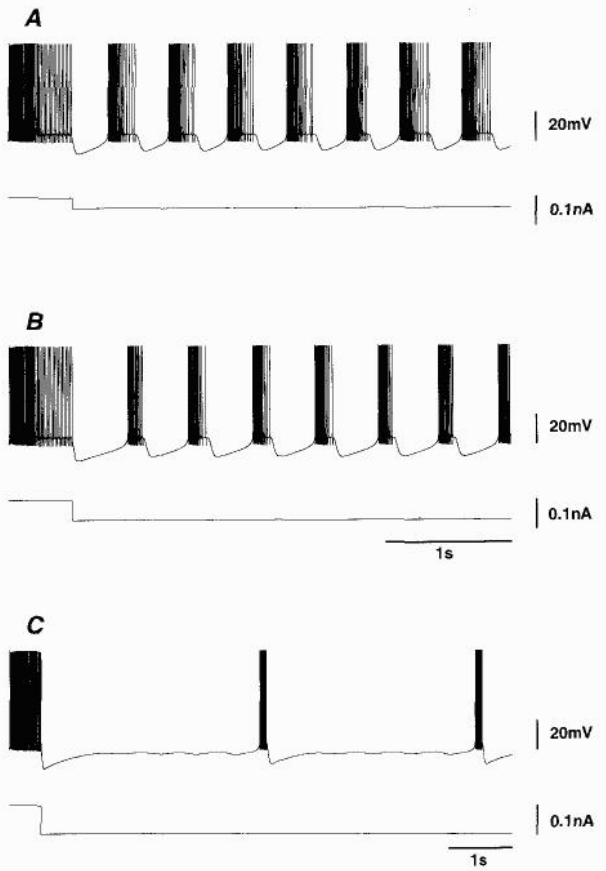

FIG. 13. Rhythmic bursting activity caused by depression of $g_{K(AHP)}$ in the standard type B model. With $\bar{g}_{K(AHP)}$ set to zero the model cell exhibited burst firing during injection of hyperpolarizing current (*A*: −0.04 nA, *B*: −0.07 nA, and *C*: −0.098 nA). The time scale is the same in *A* and *B*.

the vestibulo-ocular reflex pathway. It is, therefore, important to know the specific function of type A and type B MVNns. The MVNns receive primary vestibular afferents from the horizontal canals and project to motoneurons innervating the extra-ocular muscle rectus lateralis (Precht 1978). This suggests that at least a fraction of the MVNns mediate the horizontal VOR. Since activity of secondary vestibular neurons in the MVN can readily be recorded with extracellular microelectrodes, it is likely that they provide a major fraction of neurons successfully impaled in the intracellular recordings of Serafin et al. (1991a,b). Unfortunately, we do not know how this fraction correlates with the population of type A and type B neurons but we hope that future experiments will answer this pertinent question.

We thank Dr. Christoph Staub for many constructive discussions during the course of this study.

T. Knöpfel was supported by the Human Frontier Science Program.

Address for reprint requests: T. Knöpfel, Ciba Pharmaceuticals Division R&D, K-125.6.12, CH-4002 Basel, Switzerland.

Received 29 December 1993; accepted in final form 16 June 1994.

REFERENCES

ADAMS, P. R., BROWN, D. A., AND CONSTANTI, A. M-currents and other potassium currents in bullfrog sympathetic neurones. *J. Physiol. Lond.* 330: 537–572, 1982.

AUDINAT, E., GÄHWILER, B. H., AND KNÖPFEL, T. Excitatory synaptic potentials in neurones of the deep nuclei in olivo-cerebellar slice cultures. *Neuroscience* 49: 903–911, 1992.

BORG-GRAHAM, L. J. Modeling the nonlinear conductances of excitable membranes. In: *Cellular and Molecular Neurobiology: A Practical Approach*, edited by H. Wheal and J. Chad. New York: Oxford Univ. Press, 1991.

BROWN, D. M-currents: an update. *Trends Neurosci.* 11: 294–299, 1988.

CHURCHLAND, P. S. AND SEJNOWSKI, T. J. *The Computational Brain*, Cambridge, MA: MIT Press, 1992.

COOLEY, J. W. AND DODGE, W. A. Digital Computer Solutions for Excitation and Propagation of the Nerve Impulse. *Biophys. J.* 6: 583–599, 1966.

COULTER, D. A., HUGUENARD, J. R., AND PRINCE, D. A. Calcium currents in rat thalamocortical relay neurones: Kinetic properties of the transient, low-threshold current. *J. Physiol. Lond.* 414: 587–604, 1989.

CRÉPEL, F. AND PENIT-SORIA, J. Inward rectification and low threshold calcium conductance in rat cerebellar Purkinje cells. An in vitro study. *J. Physiol. Lond.* 372: 1–23, 1986.

DE WAELE, C., SERAFIN, M., KHATEB, A., YABE, T., VIDAL, P. P., AND MÜHLETHALER, M. Medial vestibular nucleus in the guinea-pig. Apamin-induced rhythmic burst firing: an in vitro and in vivo study. *Exp. Brain Res.* 95: 213–222, 1993.

EKEBERG, O., WALLEN, P., LANSNER, A., TRAVEN, H., BRODIN, L., AND GRILLNER, S. A computer based model for realistic simulation of neural networks 1. The single neuron and synaptic interaction, Biol. Cybern. 65: 81–90, 1991.

FRENCH, C. R., SAH, P., BUCKETT, K. J., AND GAGE, P. W. A voltage-dependent persistent sodium current in mammalian hippocampal neurons. *J. Gen. Physiol.* 95: 1139–1157, 1990.

HODGKIN, A. L. AND HUXLEY, A. F. A quantitative description of membrane current and its application to conduction and excitation in nerve. *J. Physiol. Lond.* 117: 500–544, 1952.

HODGKIN, A. L. AND KEYNES, R. D. Movements of labeled calcium in squid giant axon. *J. Physiol. Lond.* 138: 253–281, 1957.

ITO, M. Cerebellar control of the vestibulo occular reflex—around the flocculus hypothesis. *Rev. Neurosci.* 5: 257–296, 1982.

JAHNSEN, H. Electrophysiological characteristics of neurones in the guinea-pig deep cerebellar nuclei in vitro. *J. Physiol. Lond.* 372: 129–147, 1986a.

JAHNSEN, H. Extracellular activation and membrane conductances of neurones in the guinea-pig deep cerebellar nuclei in vitro. *J. Physiol. Lond.* 372: 149–168, 1986b.

JAHNSEN, H. AND LLINÁS, R. Electrophysiological properties of guinea-pig thalamic neurones: an in vitro study. *J. Physiol. Lond.* 349: 205–226, 1984a.

JAHNSEN, H. AND LLINÁS, R. Ionic basis for the electroresponsiveness and oscillatory properties of guinea-pig thalamic neurones in vitro. *J. Physiol. Lond.* 349: 227–247, 1984b.

JAHR, C. E. AND STEVENS, C. F. Voltage dependence of NMDA-activated macroscopic conductances predicted by single-channel kinetics. *J. Neurosci.* 10: 3178–3182, 1990.

KAY, A. R. AND WONG, R. K. S. Calcium current activation kinetics in isolated pyramidal neurones of the CA1 region of the mature guinea-pig hippocampus. *J. Physiol. Lond.* 392: 603–616, 198.

KIMURA, J., MIYAMAE, S., AND NOMA, A. Identification of sodium-calcium exchange current in single ventricular cells of guinea-pig. *J. Physiol. Lond.* 384: 199–222, 1987.

KNÖPFEL, T. AND GÄHWILER, B. H. Activity-induced elevations of intracellular calcium concentration in pyramidal and nonpyramidal cells of the CA3 region of rat hippocampal slice cultures. *J. Neurophysiol.* 68: 961–963, 1992.

KOCH, C. Biophysics of computation: toward the mechanisms underlying information processing in single neurons. In: *Computational Neuroscience*, edited by E. L. Schwarz. Cambridge, MA: MIT Press, 1990, p. 97–113.

KOCH, C. AND SEGEV, I. *Methods in Neuronal Modeling*. Cambridge, MA: MIT Press, 1989.

LACAILLE, J. C., MÜLLER, A. L., KUNKEL, D. D., AND SCHWARTZKROIN P. A. Local circuit interactions between oriens/alveus interneurons and CA1 pyramidal cells in hippocampal slices: electrophysiology and morphology. *J. Neurosci.* 7: 1979–1993, 1987.

LANCASTER, B. AND ADAMS, P. R. Calcium-dependent current generating the after-hyperpolarization of hippocampal neurons. *J. Neurophysiol.* 55: 1268–1282, 1986.

LANCASTER, B. AND NICOLL, R. A. Properties of two calcium-activated hyperpolarizations in rat hippocampal neurones. *J. Physiol. Lond.* 389: 187–203, 1987.

LANCASTER, B., NICOLL, R. A., AND PERKEL, D. J. Calcium activates two types of potassium channels in rat hippocampal neurons in culture. *J. Neurosci.* 11: 23–30, 1991.

LLINÁS, R. AND MÜHLETHALER, M. An electrophysiological study of the in vitro, perfused brain stem-cerebellum of adult guinea-pig. *J. Physiol. Lond.* 404: 215–240, 1988a.

LLINÁS, R. AND MÜHLETHALER, M. Electrophysiology of guinea-pig cerebellar nuclear cells in the in vitro brain stem-cerebellar preparation. *J. Physiol. Lond.* 404: 241–258, 1988b.

LYTTON, W. W. AND SEJNOWSKI, T. J. Simulations of cortical pyramidal neurons synchronized by inhibitory interneurons. *J. Neurophysiol.* 66: 1059–1079, 1991.

MATSUKAWA, L. M. AND PRINCE, D. A. Synaptic control of excitability in isolated dendrites of hippocampal neurons. *J. Neurosci.* 4: 217–227, 1984.

MOCZYDLOWSKI, E. AND LATORRE, R. Gating kinetics of Ca-activated K-channels from rat muscle incorporated into planar lipid bilayers. *J. Gen. Physiol.* 82: 511–542, 1983.

MULLINS, L. J. *An electrogenic saga: consequences of sodium-calcium exchange in cardiac muscle.* In: *Electrogenic Transport: Fundamental Principles and Physiological Implications*, edited by M. P. Blaustein and M. Lieberman, New York: Raven Press, 1984, p. 161–180.

MURI, R. AND KNÖPFEL, T. Activity-induced elevations of intracellular calcium concentrations in neurons of the deep nuclei in cerebellar slice cultures. *J. Neurophysiol.* 71: 420–428, 1994.

NEHER, E. AND AUGUSTINE, J. Calcium gradients and buffers in bovine chromaffin cells. *J. Physiol. Lond.* 450: 247–271, 1992.

PARNAS, I. AND SEGEV, I. A mathematical model for conduction of action potentials along bifurcating axons. *J. Physiol. Lond.* 295: 323–343, 1979.

PRECHT, W. *Studies of brain function: neuronal operations in the vestibular system*, New York: Springer-Verlag, 1978.

QUADRONI, R., SIMONET, J., HEPP, K., AND KNÖPFEL, T. Realistic computer simulations of medial vestibular nuclei and deep cerebellar neurons. *Soc. Neurosci. Abstr.* 18: 1207, 1992.

ROBINSON, D. A. A computational view of the oculomotor system. In:

Computational Neuroscience, edited by E. L. Schwartz. Cambridge, MA: MIT Press, 1990, p. 319–330.

RUDY, B. Diversity and ubiquity of K channels, *Neurosci.* 25: 729–749, 1988.

SAH, P., GIBB, A. J., AND GAGE, P. W. The sodium current underlying action potentials in guinea-pig hippocampal CA1 neurons. *J. Gen. Physiol.* 91: 373–398, 1988.

SALA, F. AND HERNANDEZ-CRUZ, A. Calcium diffusion modeling in a spherical neuron. *Biophys. J.* 57: 313–324, 1990.

SEGAL, M., ROGAWSKI, M. A., AND BARKER, J. L. A transient potassium conductance regulates the excitability of cultured hippocampal and spinal neurons. *J. Neurosci.* 4: 604–609, 1984.

SERAFIN, M., DE WAELE, C., KHATEB, A., VIDAL, P. P., AND MÜHLETHALER, M. Medial vestibular nucleus in the guinea-pig. I. Intrinsic membrane properties in brainstem slices. *Exp. Brain Res.* 84: 417–425, 1991a.

SERAFIN, M., DE WAELE, C., KHATEB, A., VIDAL, P. P., AND MÜHLETHALER, M. Medial vestibular nucleus in the guinea-pig. II. Ionic basis of the intrinsic membrane properties in brainstem slices. *Exp. Brain Res.* 84: 426–433, 1991b.

SERAFIN, M., KHATEB, A., DE WAELE, C., VIDAL, P. P., AND MÜHLETHALER, M. Low threshold calcium spikes in medial vestibular nuclei neurones in vitro: a role in the generation of the vestibular nystagmus quick phase in vivo? *Exp. Brain Res.* 82: 187–190, 1990.

SERAFIN, M., KHATEB, A., DE WAELE, C., VIDAL, P. P., AND MÜHLETHALER, M. Medial Vestibular nucleus in the guinea-pig: NMDA-induced oscillations. *Exp. Brain Res.* 88: 187–192, 1992.

SHELTON, D. P. Membrane resistivity estimated for the Purkinje neuron by means of a passive computer model. *Neuroscience* 14: 111–131, 1985.

SHIMAZU, H. AND PRECHT, W. Tonic and kinetic responses of cat's vestibular neurons to horizontal angular acceleration. *J. Neurophysiol.* 28: 991–1013, 1965.

SPAIN, W. J., SCHWINDT, P. C., AND CRILL, W. E. Anomalous rectification in neurons from cat sensorimotor cortex in vitro. *J. Neurophysiol.* 57: 1555–1575, 1987.

STAFSTROM, C. E., SCHWINDT, P. C., CHUBB, M. C., AND CRILL, W. E. Properties of persistent sodium conductance and calcium conductance in layer V neurons from cat sensorimotor cortex in vitro. *J. Neurophysiol.* 53: 153–170, 1985.

STORM, J. F., BORG-GRAHAM, L. J., AND ADAMS, P. R. A passive component of the afterdepolarization (adp) in rat hypocampal pyramidal cells. *Soc. Neurosci. Abstr.* 13: 502, 1987.

STUART, G. J. AND SAKMANN, B. Active propagation of somatic action potentials into neocortical pyramidal cell dendrites. *Nature Lond.* 72: 367–369, 1994.

TRAUB, R. D. AND MILES, R. *Neural Networks of the Hippocampus*. Cambridge, MA: Cambridge University Press, 1991.

TRAUB, R. D., WONG, R. K. S., MILES, R., AND MICHELSON, H. A model of a CA3 hippocampal pyramidal neuron incorporating voltage-clamp data on intrinsic conductances. *J. Neurophysiol.* 66: 635–650, 1991.

WANG, X. J., RINZEL, J., AND ROGAWSKI, M. A. A model of the T-type calcium currents and the low-threshold spike in thalamic neurons. *J. Neurophysiol.* 66: 839–850, 1991.

WONG, R. K. S., PRINCE, D. A., AND BASBAUM, A. I. Intradendritic recordings from hippocampal neurons. *Proc. Natl. Acad. Sci. USA* 76: 986–990, 1979.

YAMADA, W. M., KOCH, C., AND ADAMS, P. R. Multiple channels and calcium dynamics, methods in neuronal modeling, edited by C. Koch and I. Segev. Cambridge, MA: MIT Press, 1989, p. 97–133.